

# Light funneling mechanism explained by magneto-electric interference

Fabrice Pardo,<sup>1,\*</sup> Patrick Bouchon,<sup>1,2</sup> Riad Haïdar,<sup>2,3</sup> and Jean-Luc Pelouard<sup>1</sup>

<sup>1</sup>CNRS – Laboratoire de Photonique et de Nanostructures, Route de Nozay, 91460 Marcoussis, France  
<sup>2</sup>Office National d'Études et de Recherches Aéronautiques, Chemin de la Hunière, 91761 Palaiseau, France  
<sup>3</sup>École Polytechnique, Département de Physique, 91128 Palaiseau, France

(Dated: October 30, 2018)

We investigate the mechanisms involved in the funneling of the optical energy into sub-wavelength grooves etched on a metallic surface. The key phenomenon is unveiled thanks to the decomposition of the electromagnetic field into its propagative and evanescent parts. We unambiguously show that the funneling is not due to plasmonic waves flowing toward the grooves, but rather to the magneto-electric interference of the incident wave with the evanescent field, this field being mainly due to the resonant wave escaping from the groove.

Plasmonics, as the science of the efficient coupling of photons with free electron gas oscillation modes at the surface of metals, appears as an inescapable solution for the design and realization of optical nano antennas [1]. Numerous cutting edge applications are based on nano-antennas like biosensing [2], gas sensing [3], photovoltaic [4] or infrared photodetection [5] which exploit the intense local electromagnetic field in a confined volume [6–8]. Now, the specific matter of total photon harvesting at the nanometric scale, i.e. designing an antenna able to couple all the incident optical power with a nanoabsorber, remains challenging [1, 7–9]. The natural two-step antenna sequence (collection of light, then concentration) has been extensively studied in structures made of a metallic subwavelength grating surrounding a target [6, 10–14]. The underlying mechanism involves SPP excitation (collection) and propagation (concentration) along the grating until the coupling with the target. Such structures, though, are designed to collect light at a specific incidence angle, which is obviously a strong practical limitation.

In contrast, quasi-isotropic perfect transmission is obtained through very narrow slits drilled in a metallic membrane [15, 16]. This perfect transmission is successfully explained by a localized Fabry-Perot resonance in the slits [17]. However the funneling, namely the mechanism responsible for the *redirection and subsequent concentration of the whole incident energy flow, from the surface toward the tiny aperture of the slits*, remains unclear. Yet, a pictorial model of the underlying physics is of a key importance for the design of efficient nanoantennas.

Such a model is given by the energetic point of view [19]: Poynting vector streamlines distinctly show that the incident flow bends when reaching the metal surface, and then propagates along the interface toward the slits. This fits with the intuitive explanation, inspired by the SPP excitation process, that plasmonic waves drive the funneling sequence [20]. Furthermore, quasi-cylindrical waves were recently identified as the dominant short-range propagation process of the field amplitude along the surface of the grating [21, 22]. Nevertheless,

even if the evanescent waves are naturally assumed to concentrate the energy toward the apertures of the slits, no specific study of the light funneling has so far been carried out to our knowledge.

In this letter, we definitely unveil the funneling process, and highlight the unexpectedly limited role of the evanescent waves alone. Firstly, by analysing the particular case of a groove (for which experimental study confirm theoretical predictions [18]), we show that the evanescent waves do not carry any energy through the apertures: they simply redistribute it over the metal surface. Instead, we identify the *magneto-electric interfer-*

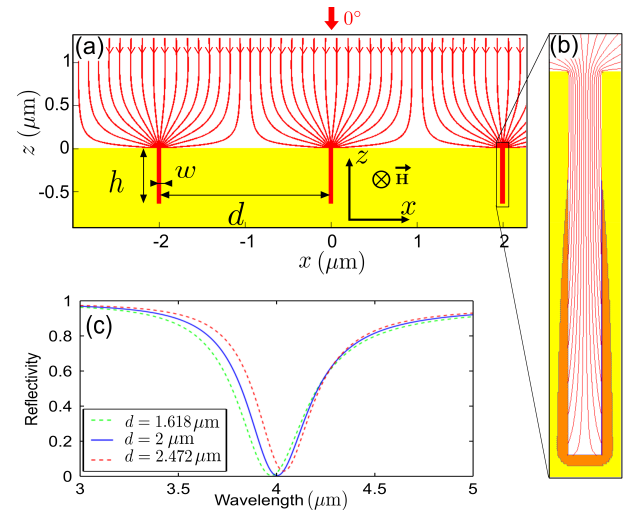


FIG. 1. (a) Poynting vector streamlines are drawn on a grating of grooves of height  $h = 640 \text{ nm}$ , width  $w = 56 \text{ nm}$  and period  $d = 2 \mu\text{m}$ . The incident energy is funneled inside the grooves. (b) Vector streamlines inside a groove. The dissipation of the energy is computed in the metallic region, it clearly appears that this dissipation occurs on the sidewalls of the grooves (orange volume), see [18] for detailed field maps. (c) Reflectivity spectra for various values of the grating period  $d = 1.618 \mu\text{m}$ ,  $d = 2 \mu\text{m}$  and  $d = 2.472 \mu\text{m}$ . The geometry of the groove is the same as before. The period has almost no influence on the resonance since it is due to the Fabry-Perot resonator inside the grooves.

ence (MEI) [23] of the incident wave with the evanescent field as the main mechanism of the funneling sequence. We then use a single interface analysis [24] to generalize our result to sub-wavelength apertures with no resonator behind. MEI also explains the broadband extraordinary transmission due to plasmonic Brewster angle that was recently published by Alù [25] (see supplemental material [18]).

Let us consider an infrared light at  $\lambda_f = 4\ \mu\text{m}$  incident onto nanometric sized grooves periodically drilled into a gold surface. Figure 1 (a) shows the geometry of the grating (width  $w = 56\ \text{nm}$ , height  $h = 640\ \text{nm}$  and period  $d$ ). The period is chosen so that there is no diffracted wave for all angles of incidence (hence  $d \leq \lambda_f/2$ ). The light is TM-polarized (transverse magnetic) and incident with an angle  $\theta$ . The dielectric function of gold is computed from the Drude model  $\varepsilon(\lambda) = 1 - [(\lambda_p/\lambda + i\gamma)\lambda_p/\lambda]^{-1}$  which is suited to the infrared spectral range for  $\lambda_p = 161\ \text{nm}$  and  $\gamma = 0.0077$  [26]. The electromagnetic analysis of this structure is done using a B-spline method [27], which can perform fast and exact computation of Maxwell equations. The Poynting-vector streamlines show how the energy flow is funneled toward the apertures, and dissipated mainly on the sidewalls of the grooves. The reflectivity of the grating is plotted in Fig. 1 (c) at normal incidence for  $d = \lambda_f/2$  and for a random value  $d = 1.618\ \mu\text{m}$ . Although the grating is structured on a tiny portion of its surface (less than 3%), it exhibits a resonance with a total absorption at normal incidence. We should highlight that  $\lambda_f$  depends only slightly on the period  $d$ . The absorption remains nearly total even for large incidence angles ( $\theta \leq 50^\circ$ ), which is adapted to light collecting systems.

In order to address the funneling mechanism, we consider the electromagnetic field in the air, and we split it into three terms. The magnetic field is expressed:

$$H_{total} = H_i + H_r + H_e, \quad (1)$$

where  $H_i$  is the incoming wave,  $H_r$  is the reflected wave, and  $H_e$  is the sum of the diffracted evanescent waves. Similar definitions can be given for the electric field components. In the rest of this letter,  $E \times H$  stands for the mean time average value of the vectorial product and is practically computed from complex amplitudes as  $\frac{1}{2}\Re(E \times H^*)$ . Thanks to the decomposition of Eq. (1), the Poynting vector can be expressed as the sum of six terms:

$$S = S_i + S_{ei} + S_r + S_{er} + S_e + S_{ir}, \quad (2)$$

with  $S_i = E_i \times H_i$ ,  $S_{ei} = E_e \times H_i + E_i \times H_e$ ,  $S_r = E_r \times H_r$ ,  $S_{er} = E_e \times H_r + E_r \times H_e$ ,  $S_e = E_e \times H_e$ , and  $S_{ir} = E_i \times H_r + E_r \times H_i$ . The terms  $S_i$  and  $S_r$  are respectively the incident and the reflected fluxes of the plane wave. The term  $S_e$  corresponds to the energy carried by the evanescent waves. The term  $S_{ei}$  corresponds to the

MEI between the evanescent and the incident fields. It is easy to prove that the six terms of equation (2) are flux conservative (null divergence) thus each of them can be considered to be an independent energy flux vector in the air. In order to simplify the discussion, we first consider an optimized device at the resonance wavelength. So we have no reflected wave, the fields  $H_r$  and  $E_r$  are null and the Poynting vector can be expressed as  $S = S_i + S_{ei} + S_e$ .

The Poynting-vector streamlines for  $S_i$ ,  $S_{ei}$  and  $S$  are plotted at two angles of incidence in Fig. (2) so that the flux of energy between two lines is constant.

At normal incidence, as expected for a propagative

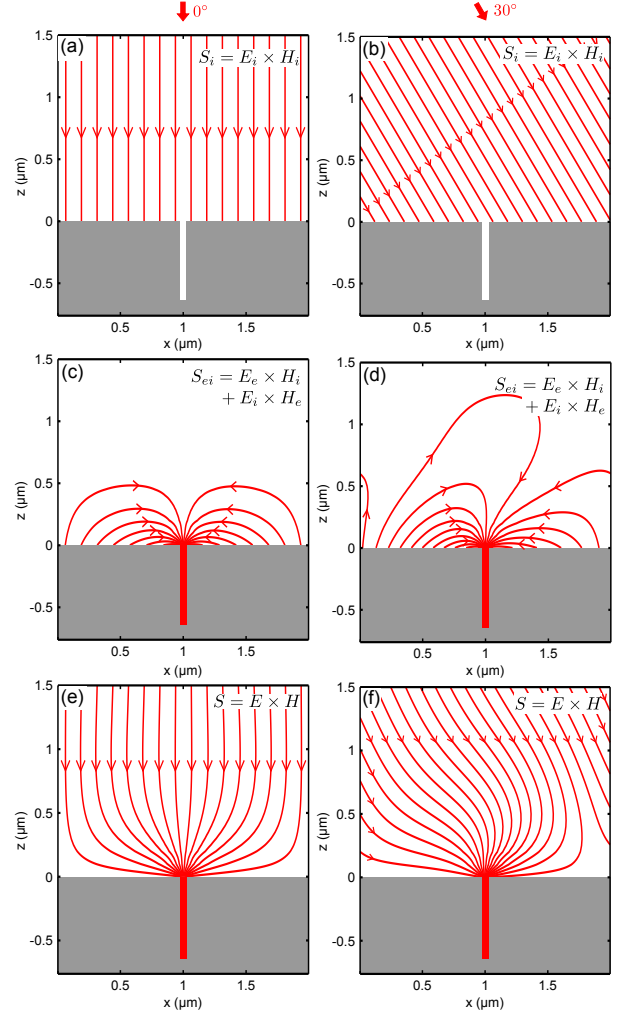


FIG. 2. Poynting-vector streamlines in one period of the slit grating for two angles of incidence  $\theta = 0^\circ$  (left column) and  $\theta = 30^\circ$  (right column) at  $\lambda = 4000\ \text{nm}$ . Streamlines of the incident wave are shown on (a) and (b). Streamlines of the interference between the incident wave and the evanescent field are shown on (c) and (d). The energy flux of the evanescent waves is negligible in this structure for  $\theta = 0^\circ$ ; refer to Fig. 3 (a) for an illustration at  $\theta = 30^\circ$ . Streamlines of the total Poynting vector are shown on (e) and (f). In both cases, the incident energy is funneled inside the groove where it is fully absorbed inside the metal.

plane wave in air, the lines for incident flux  $S_i$  are equidistant and in the propagation direction. The MEI  $S_{ei}$  lines are coming from the surface and are converging on the groove. On the metallic surface, they compensate for the flux of the incident plane wave and funnel it inside the groove. By drawing lines perpendicular to the Poynting streamlines on Fig. 2 (c), and taking in account that the predominant term in  $S_{ei}$  is  $E_e \times H_i$ , one can deduce that the evanescent wave shape is quasi-cylindrical [21, 22]. The evanescent flux  $S_e$  (not shown) carries energy 1000 times weaker and does not play an active role in the funneling for this structure at normal incidence. In Fig. 2 (e), the total flux of energy  $S$  is shown to funnel into the groove in the near-field region ( $z \lesssim 500$  nm). Eventually all the incident flux is dissipated, mostly inside the groove.

For an incidence of  $30^\circ$ , the MEI  $S_{ei}$  is still funneling the energy towards the slits (Fig. 2 (d)). But it no longer compensates for the incident flux which lines are equidistant. Indeed, in Fig. 2 (d), there are more lines going out from the metal surface on the left (10 lines) than on the right (6 lines). Nonetheless, Fig. 2 (f) shows that the incident energy gets funneled into the groove despite this asymmetry. In fact, at oblique incidence, the evanescent field carries an energy flux  $S_e$  which is no longer negligible, as shown in Fig. 3: the energy is redirected from the right side of the groove to the left side. This redistribution of the energy compensates for the dissymmetry of  $S_{ei}$  which appears in Fig. 2 (d). In conclusion  $S_e$  plays no role in the funneling, but helps to redistribute energy over the grating. This incidentally invalidates the hypothetical role of plasmonic waves, which are evanescent waves, in the funneling mechanism. As a general comment, it is interesting to point out that the MEI process is known to be responsible of the optical tunnelling (frustrated total reflection)[28]. Our study unveils its key role in a larger spectrum of near-field energy transfer phenomena.

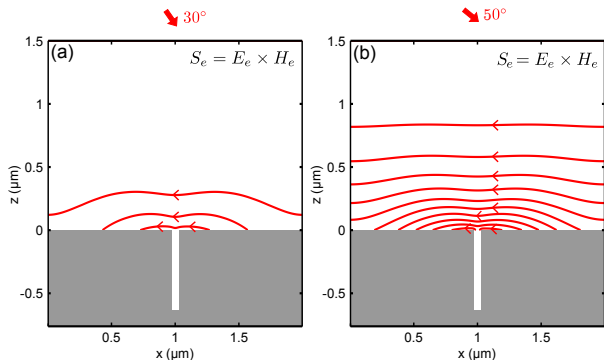


FIG. 3. Poynting-vector streamlines of the evanescent field for two angles of incidence (a)  $30^\circ$  and (b)  $50^\circ$  at  $\lambda = 4000$  nm.  $S_e$  does not play a role of funneling but redistributes the energy in the grating.

We now aim to describe the origin of the evanescent

field involved in the funneling process. The subwavelength groove behaves as a Fabry-Perot resonator. As in ref. [24], we consider the isolated single interface in two configurations: one where the incident field is a unit-amplitude plane wave in air; the other where the incident field is a wave coming from the bottom of the groove, and is unit-amplitude at the interface. In the first case (Fig. 4 (a)) the reflected wave has an amplitude  $\rho_1$  and an evanescent field  $\eta_1$ . Due to the low aperture ratio  $w/d$ , we get  $|\rho_1| \lesssim 1$  and  $|\eta_1| \ll 1$ . In the second case (Fig. 4 (b)) the transmitted wave (which corresponds to the reflected wave above) has an amplitude  $\tau_2$  and the evanescent field in the air is written  $\eta_2$ . If a unit-amplitude wave is defined as taking the value  $H_y = 1$  at the center of a groove entrance, then computation shows that evanescent amplitudes  $\eta_1$  and  $\eta_2$  are nearly equal. Due to the low aperture ratio  $w/d$ , we get  $|\tau_2| \ll 1$ .

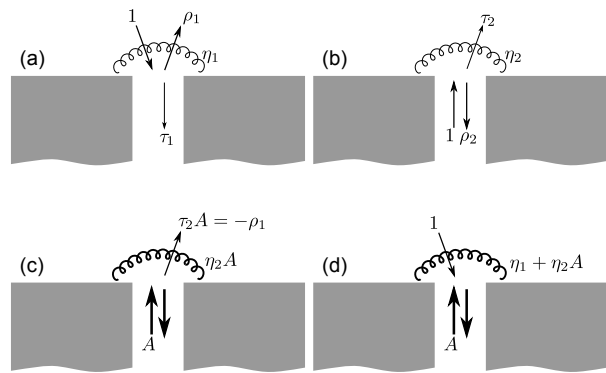


FIG. 4. Isolated single interface analysis of the metallic grating optimized to absorb all the incident light. (a) Unit plane wave from air:  $\rho_1$  is the amplitude of the reflected plane wave,  $\eta_1$  is the vector of evanescent field amplitudes. (b) Unit modal wave from bottom of grooves:  $\tau_2$  is the amplitude of the plane wave escaping in the air,  $\eta_2$  is the vector of evanescent field amplitudes. (c) Same as (b), but with the modal wave having the amplitude  $A$ . (d) Superposition of (a) and (c), showing the field amplitudes in the grating excited by a unit plane wave: the reflectivity is null and the evanescent field is dominated by the term escaping from the resonator.

At the resonance, the wave coming from the bottom of the groove has an amplitude  $A = -\tau_2^{-1}\rho_1$  so that all the amplitudes at stake in Fig. 4 (b) are multiplied by the factor  $A$ , which leads to Fig. 4 (c). The response of the grating excited by a unit-amplitude plane wave at this resonance is thus given by the superposition of amplitudes of Fig. 4 (a) and (c), shown on Fig. 4 (d). This leads to the expected null-amplitude reflected wave. Moreover, the resulting evanescent field is expressed as  $\eta_1 + \eta_2 A \simeq \eta_2 A$  because  $|\eta_1| \simeq |\eta_2|$  and  $A \gg 1$  (e.g., for the grating described in Fig. 1, one computes  $|A| \simeq 11$ ). To summarize, the wave built inside the grooves escapes in the air as both a propagating plane wave  $\tau_2 A$  and an evanescent field  $\eta_2 A$  (see Fig. 4 (c)). The propagating plane wave interferes destructively with the directly

reflected wave ( $\tau_2 A + \rho_1 = 0$ ) leading to the null reflection, and the evanescent field interferes with the incoming plane wave to funnel the energy into the groove. The two effects are of course not independent: we have no reflection because the energy is nearly fully collected in the groove. As a generalization path, it is interesting to note that this analysis still holds whatever the structure etched behind the aperture on the metal surface (rectangular slits, or more complex shapes such as in Ref.[29]).

Finally, we want to highlight that the key role played by the MEI of propagative waves with the evanescent field in the funneling mechanism is not limited to resonant structures. Let us thus consider the non-resonant case of a grating made of infinitely deep grooves, i.e. the simple isolated interface illustrated in Fig. 4(a), with a reflected wave of amplitude  $\rho_1$ . For an incidence angle of  $30^\circ$ , we get  $|\rho_1|^2 = 0.83$ : about 17% of the incident energy enters the grooves. This value is much larger than the aperture ratio  $w/d = 2.8\%$ , thus there appears to be funneling. Now, if we compare this to the situation of Fig. 4(d), the evanescent field of Fig. 4(a) is lowered by a factor  $|\eta_1 + \eta_2 A|/|\eta_1| \simeq |A| \simeq 11$ . We therefore compute that the interference of the incident wave with the evanescent field gives a funneling of about  $1/|A| \simeq 9\%$ . The missing 8% stems from the interference of the evanescent field with the reflected wave  $\rho_1$ , which paradoxically contributes to the funneling of energy inside the grooves. The key to the paradox lies here: firstly, the main contribution to the interference is  $E_e \times H_r$  ( $E_r \times H_e$  is much smaller, at least at the interface level) and, secondly, the magnetic field  $H_r$  has the sign of  $H_i$  due to the metallic reflection.

In conclusion, we have unveiled the funneling mechanism of incident light in very narrow grooves etched on a metal surface. It originates from the magneto-electric interference between the incident wave and the evanescent field, in both resonant and non resonant situations. Furthermore, this result has been generalized to any sub-wavelength aperture etched on a metal surface (whatever the structure behind it) thanks to a single interface analysis. In the resonant case, the evanescent field escaping from the apertures can lead to the full harvesting of incident photons for a broad range of incidences. From a practical point of view, this approach opens a new avenue for the design of electromagnetic resonant antennas, based on the tailoring of the escaping evanescent field.

Eventually, we have shown that evanescent waves propagating along the interface do not carry any energy through the apertures. This clearly demonstrates that the funneling is not mediated by plasmon waves at the surface.

This work was partially supported by the ANTARES Carnot project.

- \* fabrice.pardo@lpn.cnrs.fr
- [1] P. Mühlischlegel, H. Eisler, O. Martin, B. Hecht, and D. Pohl, *Science* **308**, 1607 (2005)
  - [2] A. Kabashin, P. Evans, S. Pastkovsky, W. Hendren, G. Wurtz, R. Atkinson, R. Pollard, V. Podolskiy, and A. Zayats, *Nature Materials* **8**, 867 (2009)
  - [3] N. Liu, M. Tang, M. Hentschel, H. Giessen, and A. Alivisatos, *Nature Materials*(2011)
  - [4] H. Atwater and A. Polman, *Nature materials* **9**, 205 (2010)
  - [5] M. Knight, H. Sobhani, P. Nordlander, and N. Halas, *Science* **332**, 702 (2011)
  - [6] S. Kim, J. Jin, Y.-J. Kim, I.-Y. Park, Y. Kim, and S.-W. Kim, *Nature* **453**, 757 (2008)
  - [7] J. A. Schuller, E. S. Barnard, W. Cai, Y. C. Jun, J. S. White, and M. L. Brongersma, *Nat. Mater.* **9**, 193 (2010)
  - [8] L. Novotny, *Phys. Rev. Lett.* **98**, 266802 (2007)
  - [9] L. Tang, S. E. Kocabas, S. Latif, A. K. Okyay, D.-S. Ly-Gagnon, K. C. Saraswat, and D. A. B. Miller, *Nature Photon.* **2**, 226 (2008)
  - [10] T. Thio, K. M. Pellerin, R. A. Linke, H. J. Lezec, and T. W. Ebbesen, *Opt. Lett.* **26**, 1972 (2001)
  - [11] T. Ishi, J. Fujikata, K. Makita, T. Baba, and K. Ohashi, *Jpn. J. Appl. Phys.* **44**, L364 (2005)
  - [12] Z. Yu, G. Veronis, S. Fan, and M. L. Brongersma, *Appl. Phys. Lett.* **89**, 151116 (2006)
  - [13] E. Laux, C. Genet, T. Skauli, and T. W. Ebbesen, *Nat. Phot.* **2**, 161 (2008)
  - [14] C. Genet and T. W. Ebbesen, *Nature* **445**, 39 (2007)
  - [15] J. A. Porto, F. J. García-Vidal, and J. B. Pendry, *Phys. Rev. Lett.* **83**, 2845 (1999)
  - [16] S. Collin, F. Pardo, R. Teissier, and J.-L. Pelouard, *Phys. Rev. B* **63**, 33107 (2001)
  - [17] P. Lalanne, J. P. Hugonin, S. Astilean, M. Palamaru, and K. D. Möller, *J. Opt. A* **2**, 48 (2000)
  - [18] See EPAPS Document xxx for MEI interpretation of the plasmonic Brewster effect, experimental results, field maps and scaling issues.
  - [19] H. T. Miyazaki and Y. Kurokawa, *IEEE J. Sel. Topics in Quantum Electron.* **14**, 1565 (2008)
  - [20] P. N. Stavrinou and L. Solymar, *Opt. Commun.* **206**, 217 (2002)
  - [21] H. Liu and P. Lalanne, *Nature* **452**, 728 (2008)
  - [22] X. Y. Yang, H. T. Liu, and P. Lalanne, *Phys. Rev. Lett.* **102**, 153903 (2009)
  - [23] In order to prevent any ambiguity with the traditional interference concept, namely  $\mathbf{E}_1 \cdot \mathbf{E}_2$ , we call the term  $\mathbf{E}_1 \times \mathbf{H}_2 + \mathbf{E}_2 \times \mathbf{H}_1$  the magneto-electric interference (MEI) of two waves 1 and 2.
  - [24] P. Lalanne, C. Sauvan, J. P. Hugonin, J. C. Rodier, and P. Chavel, *Phys. Rev. B* **68**, 125404 (2003)
  - [25] A. Alù, G. D'Aguanno, N. Mattiucci, and M. J. Bloemer, *Phys. Rev. Lett.* **106**, 123902 (2011)
  - [26] E. Palik, *Handbook of Optical Constants of Solids, Part II* (Academic Press, New York, 1985)
  - [27] P. Bouchon, F. Pardo, R. Haïdar, and J.-L. Pelouard, *J. Opt. Soc. Am. A* **27**, 696 (2010)
  - [28] G. S. Smith, *An Introduction to Classical Electromagnetic Radiation* (Cambridge University Press, 1997) ISBN 0521580935
  - [29] T. V. Teperik, F. J. Garcia de Abajo, A. G. Borisov,

M. Abdelsalam, P. N. Bartlett, Y. Sugawara, and J. J. Baumberg, *Nat. Photon.* **2**, 299 (2008)

[30] C. Billaudeau, S. Collin, C. Sauvan, N. Bardou, F. Pardo, and J. Pelouard, *Opt. Lett.* **33**, 165 (2008)

[31] S. Collin, F. Pardo, and J.-L. Pelouard, *Opt. Expr.* **15**, 4310 (2007)

## SUPPLEMENTAL MATERIAL

Supplementary information for the article *Light funneling mechanism explained by magneto-electric interference* (MEI). It includes the following items:

- Broadband extraordinary transmission analysis by MEI.
- Experimental results on groove gratings described in the article.
- Field maps.
- Scaling properties.

### Broadband extraordinary transmission analysis by MEI

The total funneling in the case of broadband extraordinary transmission described by Alù *et al.* [25] is illustrated on figure S2 and fully explained by MEI as shown on figure S1. In contrast with fig. 3, the evanescent fields (amongst these evanescent fields are the surface plasmon contribution), carry here strictly no energy. As a result, in both normal and Brewster incidences, MEI alone redirects all the incident energy towards the slits.

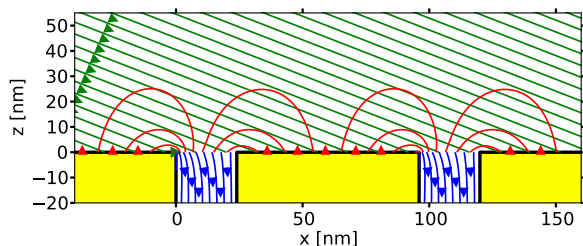


FIG. S1. Decomposition of incident energy flux of figure S2 in two terms: the incident energy flux (straight green lines), and the magneto-electric interference (MEI, curved red lines). All other terms are null. Hence, the total funneling is fully explained by MEI energy collection from the surface to the slits.

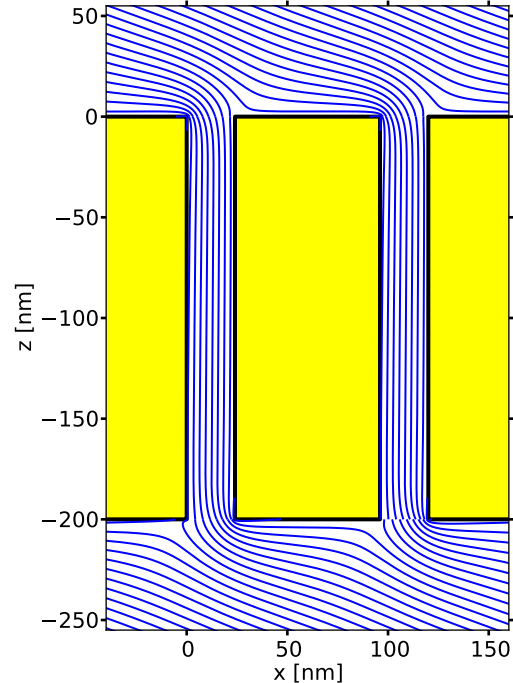


FIG. S2. Poynting vector streamlines in the broadband extraordinary transmission with parameters of Ref. [25] (wavelength  $\lambda = 759$  nm, angle of incidence  $\theta = 68.60^\circ$ , metal permittivity  $\epsilon_m = -24.7 + 1.44j$ , slit width  $w = 24$  nm, period  $d = 96$  nm, height  $h = 200$  nm). Incident wave arrive from the top left. There is strictly no resonance inside the slit and no reflexion at all. The energy flux between two lines is constant, equal to  $1/8$  of the incident energy flux on one period. Lines need to be cut around a metal bloc (here at bottom of the right slit) because of the losses.

### Experimental results

The theoretical computations presented in the article are confirmed by experimental results. To fabricate such a grating of high aspect ratio metallic grooves, we have developed a mold cast technique based on a gold electroplating. The mold in GaAs is fabricated through inductively coupled plasma reactive ion etching (ICP-RIE). A scanning electron microscope (SEM) image of the GaAs walls is shown in figure S3a, they are  $2\mu\text{m}$  high and  $150\text{nm}$  wide in a period  $d = 2.5\mu\text{m}$ . A gold electroplating is then done on the GaAs mold which is eventually chemically removed, leading to the grating of gold grooves (see SEM image in figure S3b). Measured reflectivity spectra of a TM incident wave at various angles ( $\theta = 5^\circ$ ,  $\theta = 30^\circ$  and  $\theta = 40^\circ$ ) are shown on figure S3c. They were obtained using a Fourier transform infrared spectrometer and an home-made achromatic optical system [30]. As predicted, there is an almost total extinction



of light at  $\lambda = 10.05\mu\text{m}$  which is nearly independent of the incidence angle. The measurements are in excellent agreement with the computed spectra. The corresponding funneling behavior of the poynting energy flux are shown for these three incidence angles in figure S3d-f. The reflected energy is neglected in these three cases.

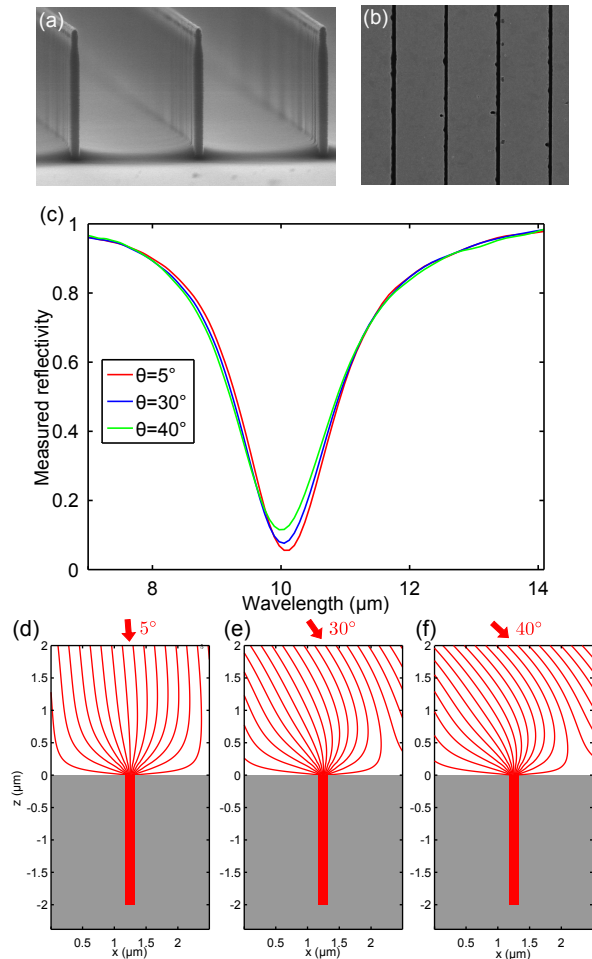


FIG. S3. (a) SEM image of the grating of GaAs walls which is used as a mold. (b) SEM image of the grating of gold slits ( $w = 150\text{nm}$ ,  $h = 2\mu\text{m}$  and  $d = 2.5\mu\text{m}$ ) obtained after an electroplating on the GaAs mold. (c) Reflectivity curves of the sample for various incident angles  $\theta = 5^\circ$ ,  $\theta = 30^\circ$  and  $\theta = 40^\circ$ . The light is TM-polarized. The resonance peak wavelength is nearly independent of the incidence angle and leads to an almost total absorption. Poynting vector streamlines at the resonance peak  $\lambda = 10.05\mu\text{m}$  for an incidence of (d)  $\theta = 5^\circ$ , (e)  $\lambda = 30^\circ$  and (f)  $\theta = 40^\circ$ . The reflected energy is neglected.

### Field maps

The magnetic and electric fields maps are shown in figure S4 a-b for the groove of width  $w = 56\text{nm}$ , depth  $h = 640\text{nm}$  and period  $d = 2\mu\text{m}$  at the resonance peak

wavelength  $\lambda_p = 4\mu\text{m}$ . The incident wave is at normal incidence and in TM polarization. The magnetic field  $H_y$  is concentrated at the bottom of the groove ( $z = -640\text{nm}$ ) while the electric field is concentrated at the aperture of the groove ( $z = 0\text{nm}$ ).

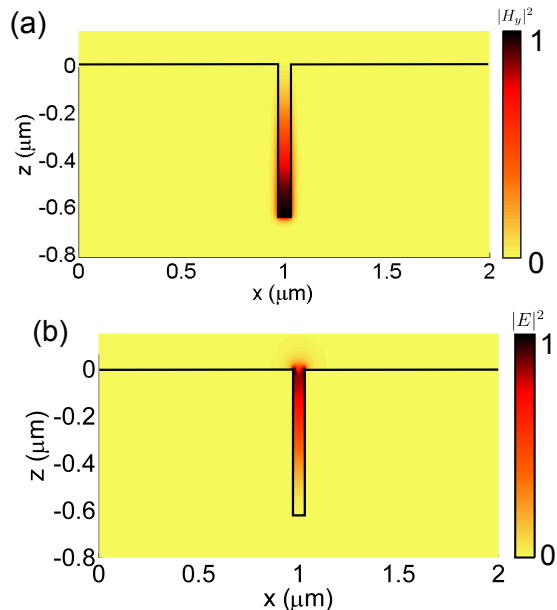


FIG. S4. Magnetic and electric fields ((a):  $|H_y|^2$ , (b):  $|E|^2$ ) in the groove of width  $w = 56\text{nm}$ , depth  $h = 640\text{nm}$  and period  $d = 2\mu\text{m}$  at the resonance peak  $\lambda_p = 4\mu\text{m}$  at normal incidence.

### Scaling properties

The dependence of the resonance peak as a function of the groove's depth  $h$  is studied in the reflectivity map plotted on figure S5. The width of the groove  $w = 56\text{nm}$  and the period of the grating  $d = 2\mu\text{m}$  are kept constant. The incident wave is TM-polarized and has an incidence of  $\theta = 0^\circ$ . There are three lines with total absorption of light appears. They correspond to the first three cavity modes inside the grooves. These resonances position as a function of the groove's depth is given by the law  $\lambda_m = 4hn_{\text{eff}}/(2m-1) + \phi$  where  $m$  is an integer standing for the resonance order,  $n_{\text{eff}}$  is the effective index of the guided mode inside the groove and  $\phi$  is the wavelength shift induced by the reflection of the guided mode on the grating surface interface. At the first order, the effective index takes a very simple form:

$$n_{\text{eff}} = 1 + \delta/w \quad (3)$$

where  $\delta$  is the skin depth of the metal [31].

The dependence of the resonance peak as a function of the groove's width is studied in the reflectivity map plotted on figure S6. The depth of the groove  $h = 640\text{nm}$  and the period of the grating  $d = 2\mu\text{m}$  are kept constant.

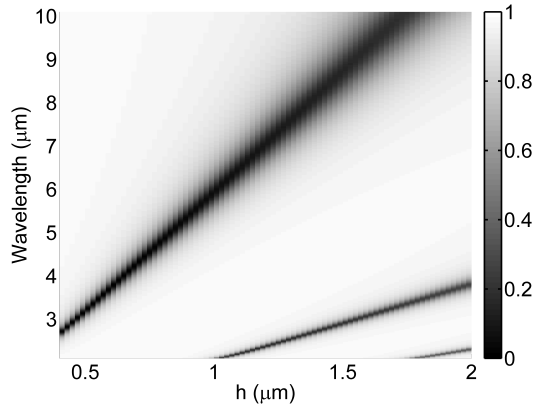


FIG. S5. Reflectivity map as a function of the groove's depth. Other parameters are kept constant (width  $w = 56\text{nm}$  and period  $d = 2\mu\text{m}$ ). The incident wave is TM-polarized and coming at normal incidence.

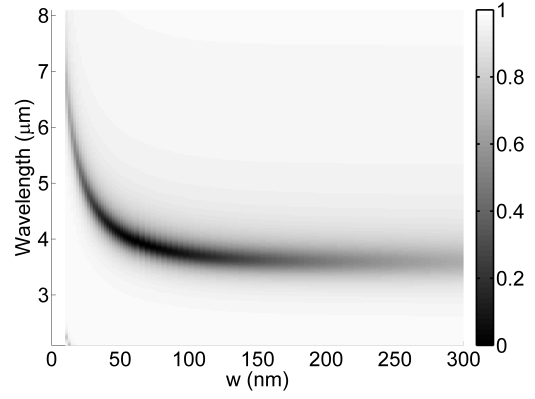


FIG. S6. Reflectivity map as a function of the groove's width. Other parameters are kept constant (depth  $h = 640\text{nm}$  and period  $d = 2\mu\text{m}$ ). The incident wave is TM-polarized and coming at normal incidence.

The inverse dependance of the resonance peak with the groove's width is coherent with the previous law given in equation 3. The dependence of the resonance peak as a function of the grating's period is studied in the reflectivity map plotted on figure S7. The depth  $h = 640\text{nm}$  and width  $w = 56\text{nm}$  of the groove are kept constant, which set the resonance peak at  $\lambda_p \simeq 4\mu\text{m}$  for subwavelength period. The reflectivity map confirms this weak influence of the period value on the resonance peak.

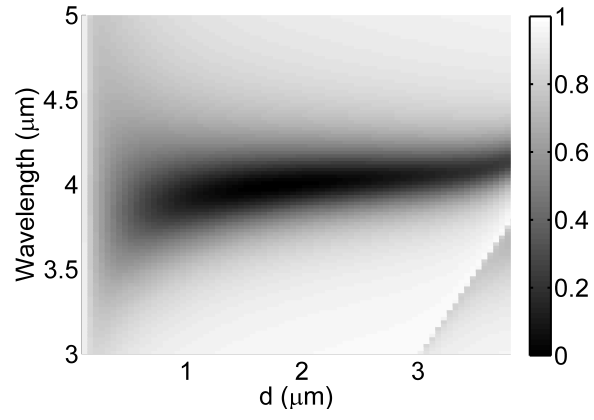


FIG. S7. Reflectivity map as a function of the grating's period. The groove's width and depth are kept constant ( $w = 56\text{nm}$  and  $h = 640\text{nm}$ ). The incident wave is TM-polarized and coming at normal incidence.